OIL PALM PLANTATION DETECTION IN INDONESIA USING SENTINEL-2 AND LANDSAT-8 OPTICAL SATELLITE IMAGERY (CASE STUDY: ROKAN HULU REGENCY, RIAU PROVINCE)

Yunita Nurmasari[1], Arie Wahyu Wijayanto[1]*

[1]Department of Computational Statistics, Politeknik Statistika STIS, Jakarta, Indonesia

*e-mail: ariewahyu@stis.ac.id

Received: 2 February 2021; Revised: 26 March 2021; Approved: 18 May 2021

Abstract. The objective of this work is to assess the capability of multispectral optical Landsat and Sentinel images to detect oil palm plantations in Rokan Hulu, Riau, one of the largest palm oil producers in Indonesia, by combining multispectral bands and composite indices. In addition to comparing two different sets of satellite images, we also ascertain which gives the best performance among the supervised machine learning classifiers CART Decision Tree, Random Forest, Support Vector Machine, and Naive Bayes. With the use of multispectral bands and derived composite indices, the best classifier achieved an overall accuracy of up to 92%. The findings and contributions of the study include: (1) insight into a set of feature combinations that provides the highest model accuracy, and (2) an extensive evaluation of machine learning-based classifiers on two different optical satellite imageries. Our study could further be beneficial for the government in providing more scalable plantation statistics.

Keywords: *remote sensing, oil palm detection, Sentinel-2, Landsat-8, supervised machine learning*

1 INTRODUCTION

Oil palm (*Elaeis guineensis*) is one of the most productive vegetable oil crops in the world (Li, Dong, Tenku & Xiao, 2015), and palm oil is used in a wide variety of food and non-food products. Due to its essential nature, global demand for the oil has grown exponentially during the last 50 years (Srestasathiern & Rakwatin, 2014). The United States Department of Agriculture (USDA) officially stated that Indonesia is the main palm oil-producing country (USDA, 2020). In 2019, it produced 42.5 million tons, or 58 percent of the global supply (McCarthy, 2020). The USDA maps palm oil production by province and shows that Riau province has the largest production percentage. Statistics Indonesia (BPS) also noted that in 2019 Indonesia palm oil production reached 45.86 million tons, with Riau producing 9.12 million tons (BPS 2020). Figure 1-1 shows the USDA Indonesia oil palm map.

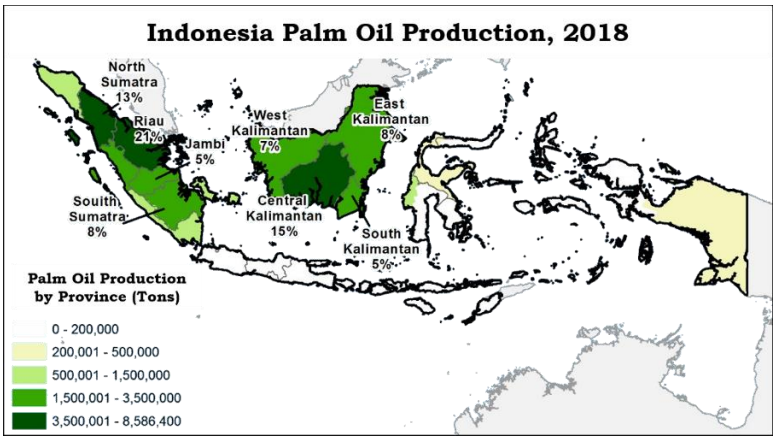

Figure 1-1: Indonesia Oil Palm Map (USDA, 2020)

http://dx.doi.org/10.30536/j.ijreses.2021.v18.a3537

Collecting information on oil palm plantations is undoubtedly important for monitoring the changes in oil palm areas and also predicting the amount of oil palm production in a region. The utilisation of remote sensing technology as an alternative to traditional methods has allowed many researchers to find various techniques and ways to increase oil palm tree inventories (Mubin, Nadarajoo, Shafri & Hamedianfar, 2019). It is easy to detect oil palm trees through satellite imagery because of their unique characteristics and morphology (Shafri, Hamdan & Saripan, 2011); for example, the trees have a star-shaped canopy if viewed from above. The existing conventional approaches to the detection of oil palm areas are mainly in the form of plantation surveys. However, such approaches are labour-intensive and involve more time and costs, especifically for large plantation areas. The remote sensing technique offers a new alternative for detecting oil palm areas with less effort, cost, and processing time. Moreover, currently the world is being hit by the Covid-19 pandemic, meaning everyone is required to reduce outdoor activities. Remote sensing techniques can minimise human contact and also provide faster and more accurate results.

Various research has been conducted related to oil palm plantation detection. Multiple techniques have been developed to map oil palm land-cover, using medium or high-resolution satellite imagery. Several studies have revealed that detecting oil palm land-cover can be done using spectral information from remote sensing data. For example, Shafri et al. (2011) demonstrated the use of CNN deep learning for detecting and counting oil palm plantations using RGB spectral bands from the WorldView-3 satellite. In addition, Vadivelu, Ahmad and Choo (2014) employed Maximum Likelihood and Support Vector Machine (SVM) machine learning for detecting and classifying oil palm plantations using spectral bands from the LANDSAT-5 TM satellite. In relation to areas in Indonesia, Lee, Wich, Widayati and Koh (2016) utilised CART and Random Forest machine learning to detect oil palm plantations using multispectral bands from the Landsat 8 TOA satellite. In further exploration, the researchers combined multispectral bands with composite indices such as the vegetation indices NDVI, EVI, and SAVI. Mansor and Sarker (2015) employed Maximum Likelihood and the Artificial Neural Network (ANN) for oil palm classification based on age groups using composite indices from the WorldView-2 satellite. Several kinds of research have been conducted in study areas in Indonesia. Dwinita and Murti (2016) demonstrated the use of Linear Regression to detect oil palm plantations using RGB bands, the NIR band, and the NDVI vegetation index from the SPOT-5 satellite. Furthermore, Tridawati and Darmawan (2015) utilised Maximum Likelihood, Minimum Distance, and SVM for oil palm plantation detection using multispectral bands and the NDVI vegetation index from the Landsat-8 OLI satellite. Freudenberg, Nölke, Agostini, Urban, Wörgötter and Kleinn (2019) employed CNN U-Net deep learning for the detection of oil palm plantations using RGB bands, the NIR band, and the NDVI vegetation index from the WorldView-2 satellite. These studies used different remote sensing approaches in terms of satellite type, spectral band, composite index, and algorithm. Different satellites use different resolutions. In Malaysia, there have been many studies related to the utilisation of remote sensing to detect oil palm plantation areas, using various approaches. However, there are unfortunately still few studies related to Indonesia.

One of our main contributions in this study compared to previous research is the utilisation of multiple satellite images, including Sentinel-2 satellite imagery, which has a higher spectral band resolution of up to 10 meters. Previously, use of this satellite was chargeable, but since 2019 it has been free. We also used Landsat-8 surface reflectance satellite imagery and combined the multispectral bands with various composite indices. Those used were the NDVI and EVI vegetation indices. The NDBI building index was also used to classify the built-up land class. We used four popular supervised machine learning algorithms to detect oil palm plantations: the CART decision tree, Random Forest, SVM, and Naive Bayes. Finally, we chose the best model from the four algorithms, which used with used with the Student's T-test.

This paper aims to: (1) evaluate the use of two optical satellite images with different resolutions; (2) identify the best feature composition; and (3) ascertain the best classifier for detecting oil palm plantations from each satellite image.

2 MATERIALS AND METHODOLOGY

2.1 Study area

Riau is the largest oil palm producing province in Indonesia. According to BPS (2019) the country's palm oil production was 45.86 million tons, of which Riau Province had the highest share, with 9.12 million tons. Rokan Hulu is the regency with the largest oil palm plantation area among the districts and cities of Riau, with 480,665 hectares. Therefore, we chose Rokan Hulu Regency as the region of interest (ROI). The study area was located at latitude 1°14 ' to 2°45' and longitude 100°17 ' to 101°21'. Figure 2-1 shows a map of the Regency.

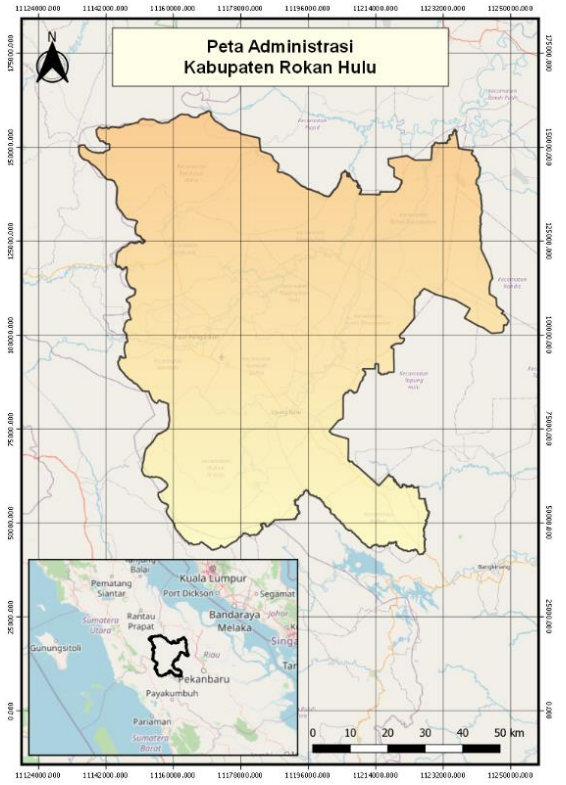

Figure 2-1: Map of Rokan Hulu Regency Riau, Indonesia

2.2 Data Collection

We searched for Sentinel-2 MSI and Landsat-8 Surface Reflectance Tier 1 satellite imageries from 1st June to 31st August 2019 from the GEE data catalog. GEE is a cloud computing platform that providing planetary-scale geospatial analysis. It has access to a large amount of imagery data from various satellites, which are continuously updated. The function of GEE is to provide images needed for analysis and also to perform image pre-processing, including the cloud filtering and cloud masking stages. We filtered the images by setting the cloud coverage percentage at less than 20 percent and sort them from the smallest The Sentinel-2 satellite image collection was obtained with cloud percentages of 7.34%, 1.26%, and 0.05%. The Landsat-8 satellite image collection had cloud percentages of 18.36%, 15.92%, and 12.44%. Figures 2-2 and 2-3 show the filtered imagery of the Sentinel-2 and Landsat-8 satellites.

Figure 2-2: Sentinel-2 satellite imagery of Rokan Hulu

Figure 2-3: Landsat-8 satellite imagery of Rokan Hulu

The filtered images were then entered into the cloud masking stage, during which the cloud-covered pixels were replaced with null, meaning the satellite images were ready to be processed.The sample points were taken with an visual estimate by comparing the Sentinel-2 and Google satellite imagery as a selection guide. We divided the main target classes into oil palm and non-oil palm. The oil palm class was defined as all oil palm plantations, including young and mature ones. The non-oil palm class was divided into forest, open field (non-oil palm non-forest), bare soil, built-up area (consisting of roads and buildings), and water. This was done to make the non-oil palm class less heterogeneous, in order to maximise the performance of machine learning. The sample size was 1800 points randomly distributed around Rokan Hulu, with each class having the same size (balance) of 300 points. The sample points were used for both Sentinel-2 and Landsat 8 satellite imagery. Table 2-1 shows the number of sample points of each predicted class, while Figure 2-4 shows the object comparison between the Sentinel-2 imagery in true colours and the Google satellite imagery.

Table 2-1: List of the six predicted classes

Class	Class name	Sample points
1	Oil Palm	300
2	Forest	300
3	Open field	300
4	Bare soil	300
5	Built-up area	300
6	Water	300
	Total	1800

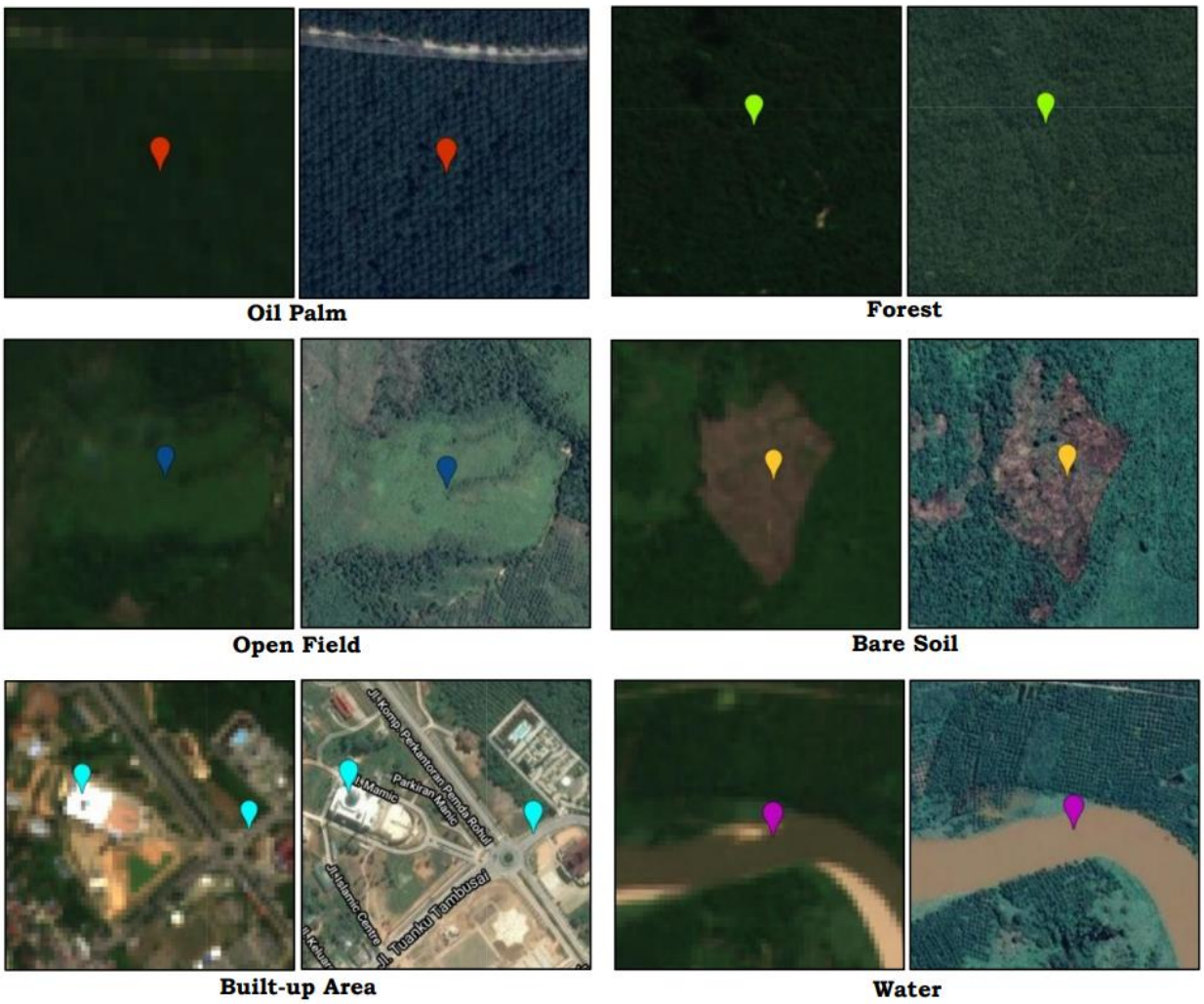

Figure 2-4: Comparison of Sentinel-2 satellite imagery (left) and Google satellite imagery (right) as a guide for each target class

2.3 Feature collection

The feature collection consisted of selected multispectral bands and composite indices as predictor variables. Sentinel-2 has spectral bands at three different spatial resolutions with ground sampling distances of 10, 20, and 60 meters, while Landsat-8 has the same spatial resolution (30 meters) for all the spectral bands. Finer resolution levels effectively improve the classification accuracy of land use classes (Chen, Li & Wang, 2010). Based on previous experiments (Shafri et al., 2011; Vadivelu et al., 2014; Lee et al., 2016; Dwinita et al., 2016; Freudenberg et al., 2019), the multispectral bands (from both satellites) of Red, Green, Blue, NIR, SWIR 1, and SWIR 2 we only used as predictor variables in this study. These bands are the basic spectral bands that are used by Sentinel-2 and Landsat-8, which will form various composite indices.

A composite index is an index composed of the transformation of multiple satellite spectral bands. Various spectral indices are determined to infer land cover properties; for example, vegetation health, burnt areas, and fire severity. In other words, the index is usually specified for a specific task (Hoeser & Bachofer, 2020). For example, green vegetation objects absorb more infrared waves (NIR) than other spectral bands, so the NIR band is one of the components in various vegetation index formulas. Since the proposed method was oriented towards green segmentation, i.e. oil palm trees, a vegetation index was an appropriate feature for this purpose. A

vegetation index (VI) is an index composed of multiple satellite bands calculated using a specific spectral transformation (Wijayanto, Triscowati & Marsuhandi, 2020). The NDVI and EVI vegetation indices have been widely used in previous studies related to the detection and classification of oil palm plantations (Lee et al., 2016; Mansor et al., 2015; Dwinita et al., 2016; and Freudenberg et al., 2019). The Normalized Difference Vegetation Index (NDVI) is a transformation using the NIR and Red bands. It provides the ability to evaluate the existence of live vegetation in the observation target (Wijayanto et al., 2020). The Enhanced Vegetation Index (EVI) is a transformation using the NIR, Red, and Blue bands. This composite index simultaneously corrects the NDVI results for atmospheric influences and soil background signals, and is especially accurate in areas of dense canopy (Solutions HG, 2013). In addition, another composite index is also needed to distinguish the built-up area class. One of the composite indices that is widely used to detect buildings is the Normalized Difference Built-up Index (NDBI) (Marsuhandi, Triscowati & Wijayanto, 2020). Three composite indices (NDVI, EVI, and NDBI) were employed in the research to map land cover in ROI. The generalised expression of these spectral indices is as follows:

$$NDVI = \frac{NIR - Red}{NIR + Red} \quad (2\text{-}1)$$

$$EVI = 2.5 \times \frac{NIR - Red}{1 + NIR + (6 \times Red) - (7{,}5 \times Blue)} \quad (2\text{-}2)$$

$$NDBI = \frac{SWIR - NIR}{SWIR + NIR} \quad (2\text{-}3)$$

Table 2-2 gives a list of the selected multispectral bands and composite indices used in this paper.

Table 2-2: List of selected multispectral bands and composite indices

Name		Description
Sentinel-2	**Landsat-8**	
B2	B2	Blue
B3	B3	Green
B4	B4	Red
B8	B5	NIR
B11	B6	SWIR 1
B12	B7	SWIR 2
NDVI		Index
EVI		Index
NDBI		Index

2.4 Methods

The research stage was divided into pre-processing, processing, and validation stages. We performed a pre-processing stage in GEE because of its functions which include cloud filtering and cloud masking stages. In the processing stage, we used Google Collaboratory Notebook (GCN) with Python API. The functions of GCN are to identify the features of multispectral bands and composite indices; divide the data set into training and testing data; train the training data for each supervised classification algorithm; perform validation and accuracy assessments; and show the visualisation. With GCN, analysis can be made in more ways because there are many packages that are not included in GEE. In general, the methodology of the study is illustrated in Figure 2-5.

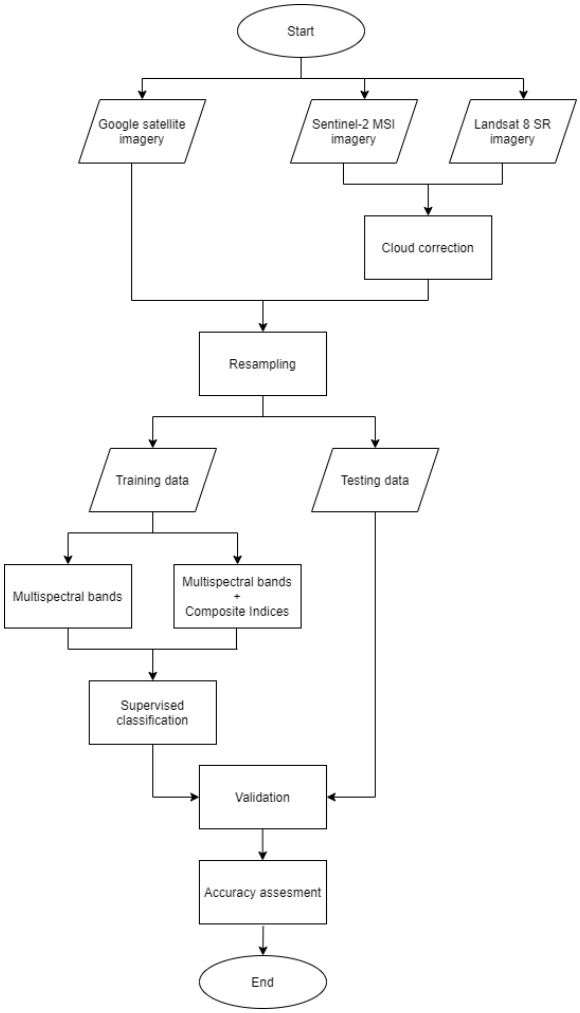

Figure 2-5: Overall Methodology.

The preprocessing stage involved various steps. First, Sentinel-2 and Landsat-8 satellite imageries were taken based on the time frame specified in the previous section. The next step was cloud correction, in which the satellite images were filtered and masked to obtain ready-to-process images. After performing the cloud filtering, the results were sorted based on the smallest cloud percentage. We next conducted the cloud masking stage because cloud was not included as the predicted class.

In the processing stage, each image was processed with widely used supervised classification algorithms: Classification and Regression Trees (CART), Random Forest, Support Vector Machine (SVM), and Minimum Distance. The CART Decision Tree is increasingly being applied for the analysis and classification of remotely sensed data. For example, it has been successfully used for multispectral imagery classification (Abdel-Hamid, Dubovyk, El-Magd & Menz., 2018). CART model representation is a binary tree, in which each node of the decision tree structure makes a binary decision that separates either one or various classes from the remaining ones (Zhang et al., 2018). Creating a CART model involves selecting input variables and splitting points on those variables until a suitable tree is constructed (Zhang et al., 2018). We set the model with a weighted class. The Random Forest algorithm is an extension of the CART algorithm by applying the bootstrap aggregating (bagging) method and random feature selection (Triscowati, Sartono, Kurnia, Domiri & Wijayanto, 2019). This method can process large amounts of data, involving many variables in the modeling process, which are sensitive to neither overfitting nor multicollinearity (Triscowati et al., 2019). It consists of several decision trees built using random vectors. The more the dataset increases, the greater the number of trees created. We also set the model with a weighted class. Support Vector Machine (SVM) is a non-parametric statistical learning approach, which can resolve complex class distribution in high dimensional feature spaces (Abdel-Hamid et al., 2018). SVM can solve problems such as overlapped objects with other classes by finding the best hyperplane and maximising the distance between classes. We used C SVC as the SVM type, with the linear kernel type, and set the cost parameter to 1. Minimum Distance is a simple algorithm (distance metric) used as a classifier for pattern recognition problems (Santucci, 2017). We set Mahalanobis as the distance metric.

We used K-Fold cross-validation as a validation method to avoid overfitting results. This method partitions the data

sample into two complementary subsets, one for analysis (called the training data), and the other for validating the analysis (called the testing data). To reduce variability, multiple rounds of cross-validation were performed using different partitions; this parameter is called k. Finally, the validation results were averaged over the rounds to give an estimate of the model's predictive performance. In this study, we set k equal to 10 to split the training and testing data.

Performance assessments were included of some metrics, such as accuracy, precision, recall (sensitivity), and f1-score. Accuracy was used to observe the closeness between the predicted and actual value. Precision shows the level of accuracy between the information requested by the user and the answers given by the model. Recall shows the success level of the model in recovering information. The F1-score is the harmonic average of precision and recall. In this study, we used the overall accuracy and f1-score measures for all the experiments to evaluate the performance of the method. We used overall accuracy (OA) to indicate the optimisation performance of each classification model and the f1-score to describe class-specific accuracy (Chen et al., 2020). The F1-score and OA ranged from 0 to 1 and tended to be at their best when approaching 1. The computation for the OA and F1-score was as follows:

$$Overall\ Accuracy = \frac{Precision + Recall}{2} \quad (2\text{-}4)$$

$$F1\text{-}score = \frac{2\ x\ Precision\ x\ Recall}{Precision + Recall} \quad (2\text{-}5)$$

3 RESULTS AND DISCUSSION

3.1 Data exploration

The boxplot exploration in Figures 3-1 and 3-2 shows information about the spectral bands and composite indices for both the Sentinel-2 and Landsat-8 satellite images. From the box diagram of the Sentinel-2 imagery, it can be seen that RGB bands do not have a significant effect on differentiating between the target classes. The NIR band is mostly absorbed by the open field class, followed by the oil palm and forest classes. This indicates that the NIR band is mostly absorbed by green vegetation. SWIR 1 is successful in differentiating the bare soil class, characterised by the high mean. SWIR 2 has the same result, but it is not as significant as the SWIR 1. If we observe the composite index, NDVI has a high value for the oil palm, forest, and open field classes. The EVI index also gives a high value for the three classes, but not as high as NDVI. This shows that the use of the NDVI and EVI composite indices is appropriate for differentiating between vegetation classes. However, none of the vegetation indices is able to differentiate the oil palm class, especially from the forest class, which has a high similarity. The NDBI index gives a high value for the bare soil and built-up area classes. However, this is unimportant, because the main focus is the oil palm class. Therefore, NDBI is appropriate for differentiating non-oil palm areas.

Similar results are also shown in the box diagram of the Landsat-8 imagery. However, some classes have a wide inter-quartile range. This is because some of the sample points are covered in cloud (as explained earlier, cloud-covered pixels will have no value, and the Landsat-8 imagery also contains a sizable percentage of cloud). Figures 3-1 and 3-2 show the boxplots of the spectral bands and composite indices for each satellite

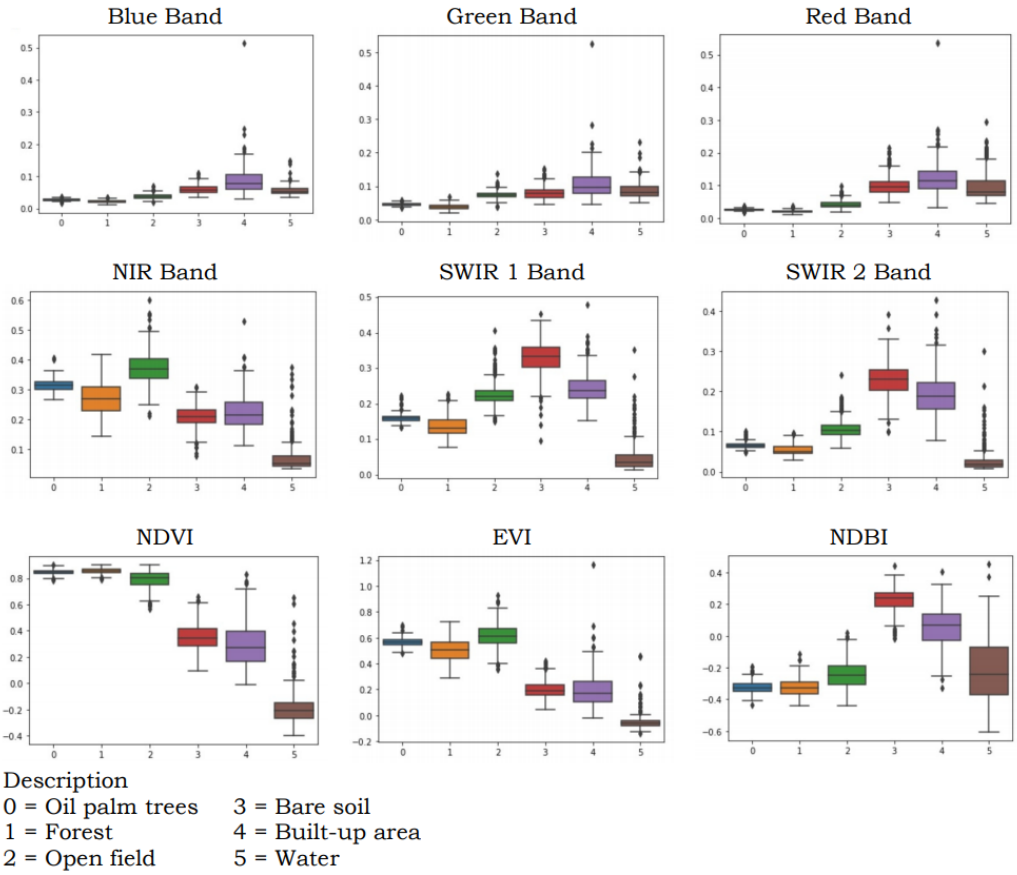

Figure 3-1: Boxplot of spectral band and composite index from Sentinel-2 images.

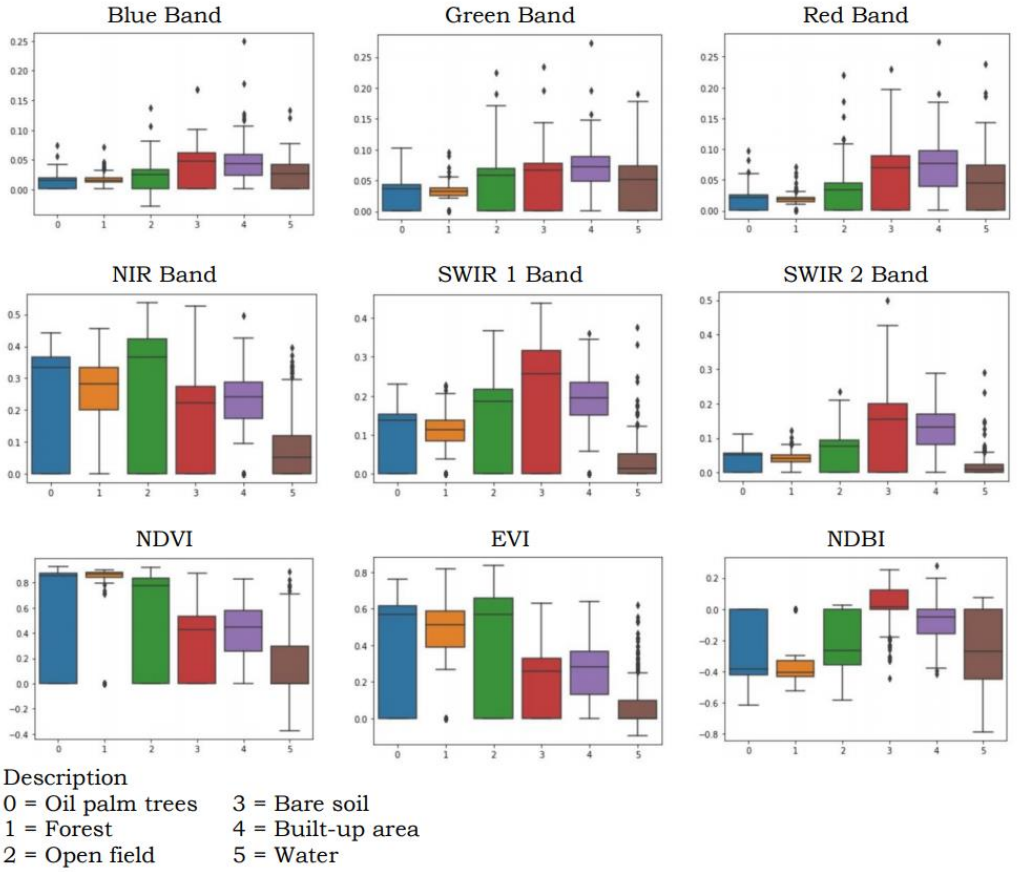

Figure 3-2: Boxplot of spectral band and composite index from Landsat-8 images

3.2 Classification results

The trained model was implemented across all the Rokan Hulu area. Sentinel-2 satellite imagery produced a better view because it had a low cloud percentage (as explained earlier). Meanwhile, in the same period, the Landsat-8 imagery contains a high cloud percentage, making the images incomplete because the pixels that contained the cloud were removed. Moreover, the Sentinel-2 satellite imagery has a more detailed view due to its higher spectral band resolution (10 meters for RGB & NIR; 20 meters for SWIR) than the Landsat-8 imagery (30 meters for all spectral bands). Figures 3-3 and 3-4 show classified maps for each algorithm in the Sentinel-2 and Landsat-8 imagery.

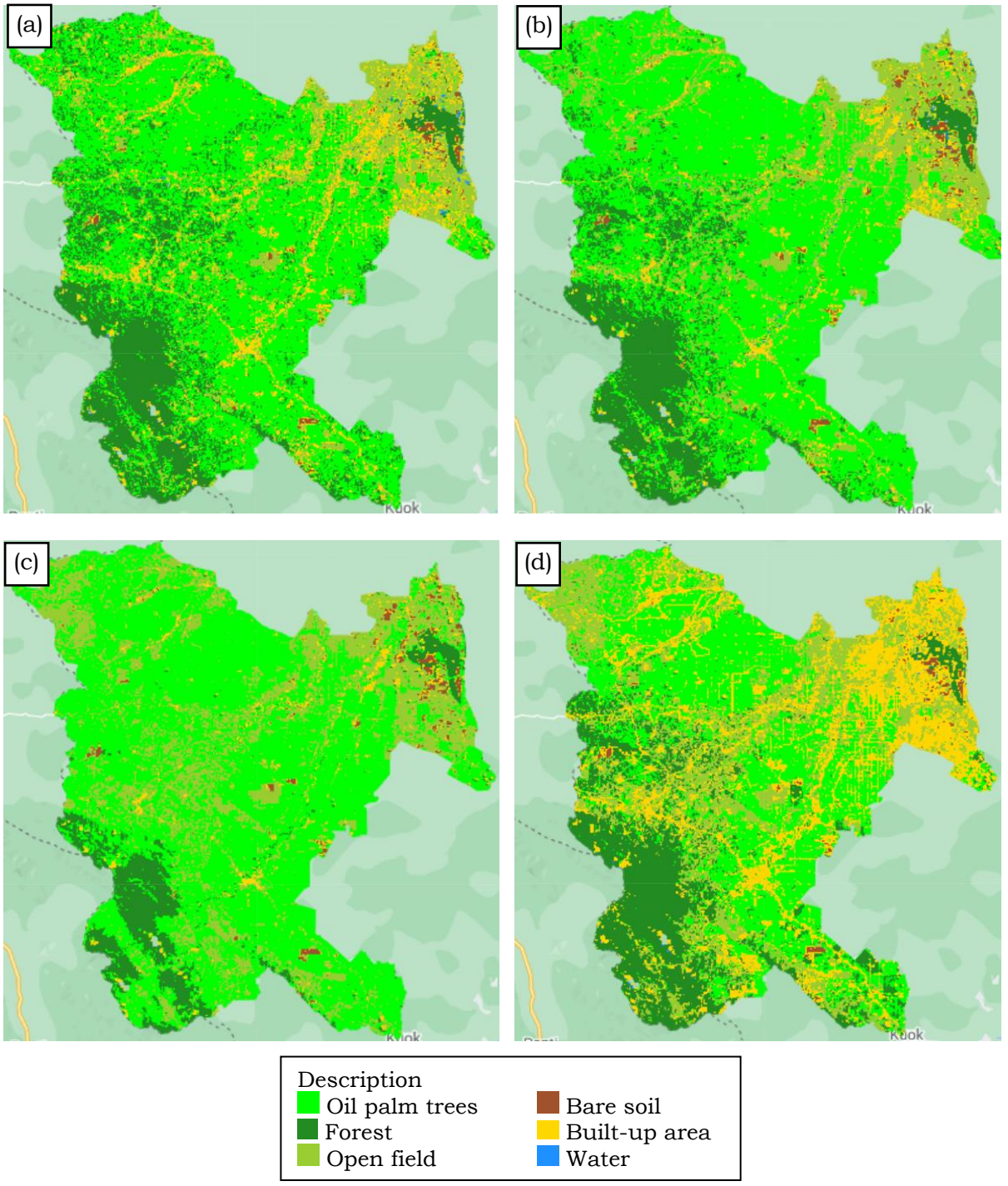

Figure 3-3: Classification results for Sentinel-2: (a) CART Decision Tree; (b) Random Forest; (c) SVM; (d) Naive Bayes

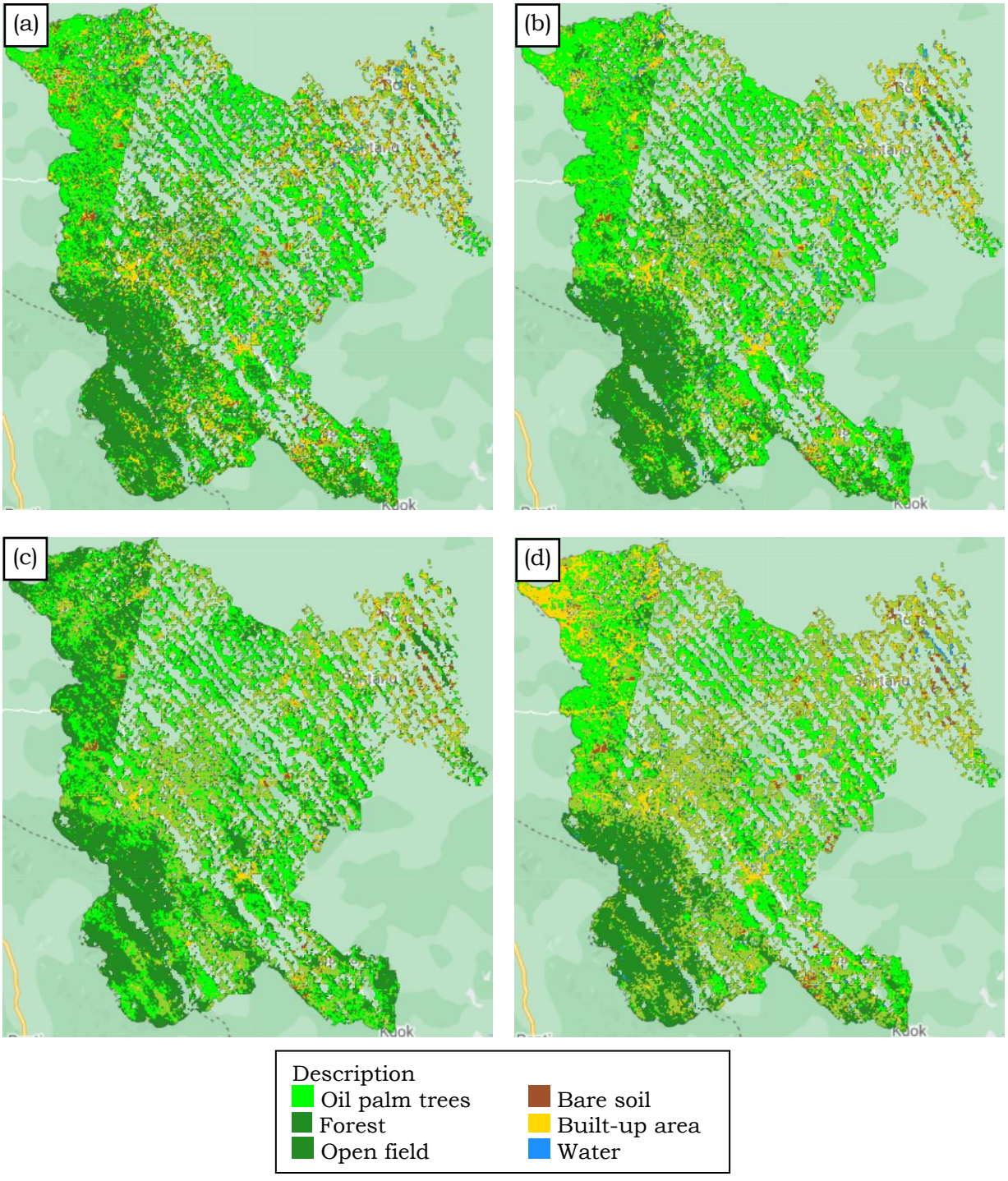

Figure 3-4: Classification results for Landsat-8: (a) CART Decision Tree; (b) Random Forest; (c) SVM; (d) Naive Bayes

3.3 Validation and statistics test

Instead of split validation, we used k-fold cross-validation as a validation method to avoid overfitting results, with k = 10 fold with a random selection of sample points. Since the method produces fluctuating numbers, we performed a running code 30 times. We recorded the results for each running code to obtain the mean and standard deviation. The metric assessment used was accuracy and F1-score. Table 3-1 shows the subsequent output for each supervised algorithm, and Figure 3-5 shows the bar chart of accuracy and the f1-score mean.

Table 3-1: Model performance comparison.

Satellite	Model	Accuracy		F1-score	
		Mean	Standard deviation	Mean	Standard deviation
Sentinel-2	CART	0.89	0.0072	0.89	0.0074
	Random Forest	**0.92**	0.0057	**0.92**	0.0060
	SVM	0.87	0.0071	0.86	0.0069
	Naive Bayes	0.87	0.0074	0.87	0.0071
Landsat-8	CART	0.61	0.0076	0.62	0.0074
	Random Forest	**0.65**	0.0119	**0.66**	0.0116
	SVM	0.55	0.0093	0.52	0.0105
	Naive Bayes	0.52	0.0129	0.48	0.0115

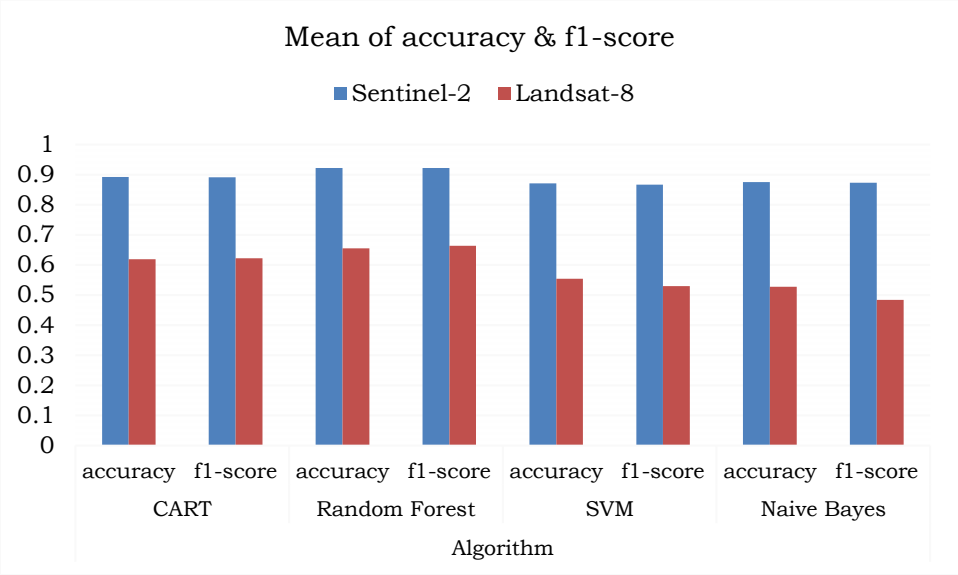

Figure 3-5: Bar chart of accuracy and f1-score mean.

Based on the table and graph above, the Sentinel-2 imagery has a higher mean of accuracy and f1-score than that of Landsat-8. The Sentinel-2 imagery also gives lower SD than that of Landsat-8. This can be caused by several factors. First, the Sentinel-2 imagery has less noise (cloud) than that of Landsat-8 (as explained in the materials and methodology section). Cloud cover has an effect on the sample points, so may cause lower accuracy. Second, the Sentinel-2 imagery has a higher resolution than that of Landsat-8. The higher the resolution, the smaller the pixel size. The relatively small pixel size can depict parts of the earth's surface in detail and more finely, thus increasing the accuracy.

Based on the model, the Random Forest algorithm produces the highest accuracy compared to other classification algorithms. In the Sentinel-2 imagery, Random Forest produces an average accuracy of 92 percent and an average f1-score of 0.92, while in the Landsat-8 imagery, it produces an average accuracy of 65 percent and an average f1-score of 0.66. However, a statistical test is needed to determine that Random Forest is the best algorithm.

There are two types of statistical measurements: parametric and non-parametric statistics. The test we used in this study was the parametric statistics Student's T-test.

Student's T is one of the most common techniques used to test whether there is a difference between two sample means. It focuses on the random forest algorithm output. For 30 experimental outputs, Random Forest output will be tested in pairs with each other algorithm output. We used an independent t-test because the sample points were processed independently of for each algorithm. In parametric statistics, certain conditions must be fulfilled: the data should be normally distributed and their variance homogeneous. However, for two independent groups, variance similarity is not an absolute requirement. Table 3-2 shows the normality test results for the Sentinel-2 imagery and Table 3-3 that of Landsat-8.

Table 3-2: Normality test results for Sentinel-2.

Model	Shapiro-Wilk	
	P-value Accuracy	P-value F1-score
CART	0.5733	0.2530
Random Forest	0.1790	0.5605
SVM	0.5475	0.9991
Naive Bayes	0.2517	0.3597

Table 3-3: Normality test results for Landsat-8.

Model	Shapiro-Wilk	
	P-value Accuracy	P-value F1-score
CART	0.2530	0.2530
Random Forest	0.1790	0.5605
SVM	0.5475	0.9991
Naive Bayes	0.2517	0.3597

We used the Shapiro-Wilk test to check the data normality with the null hypothesis: the data were normally distributed. Tables 3-2 and 3-3 show that all the groups have a p-value above 0,05, meaning the null hypothesis is accepted. We can conclude that for both the Sentinel-2 and Landsat-8 imageries, the average accuracy and f1-scores for each model are normally distributed.

Furthermore, variance similarity was tested with Bartlett's test. The statistical test used tested that the variances were equal for all the samples to the null hypothesis: variance between the two groups was equal. Because the Random Forest model is our focus, this model will be tested with each other model. Table 3-4 shows the Bartlett test results for the Sentinel-2 imagery and Table 3-5 those of the Landsat-8 imagery.

Table 3-4: Bartlett's test results for Sentinel-2.

Model	Bartlett (Random Forest)	
	P-value Accuracy	P-value F1-score
CART	0.2236	0.2707
SVM	0.2547	0.4532
Naive Bayes	0.1827	0.3932

Table 3-5: Bartlett's test results for Landsat-8.

Model	Bartlett (Random Forest)	
	P-value Accuracy	P-value F1-score
CART	0.0186	0.0253
SVM	0.2070	0.2531
Naive Bayes	0.6438	0.5600

Tables 3-4 and 3-5 show that all the groups except for the CART model in Landsat-8 have p-values above 0.05, so the null hypothesis is accepted. Therefore, we can conclude that all the models have an equal variance with the Random Forest model, apart from the CART model in Landsat-8. However, it should be remembered that variance similarity is not an absolute requirement.

Finally, the Student's T-test was used to ensure that Random Forest was the best model. An independent t-test was conducted in pairs between the Random Forest model with each other model with a null hypothesis: there was no difference on average between the two groups. Table 3-6 shows the Student's T-test results for

the Sentinel-2 imagery and Table 3-7 those for the Landsat-8 imagery.

Table 3-6: Student's T-test results for Sentinel-2

Model	Student's T (Random Forest)	
	P-value Accuracy	P-value F1-score
CART	3.37E-10	6.80E-11
SVM	2.18E-21	4.06E-23
Naive Bayes	9.44E-20	4.29E-19

Table 3-7: Student's T-test results for Landsat-8

Model	Student's T (Random Forest)	
	P-value Accuracy	P-value F1-score
CART	1.05E-02	7.01E-07
SVM	1.53E-25	8.19E-34
Naive Bayes	1.41E-27	5.68E-40

Tables 3-6 and 3-7 show that all groups have a very low p-value below 0,05, so the null hypothesis was rejected. We can therefore state that Random Forest was the best model for both Sentinel-2 and Landsat-8 imageries.

3.4 Random Forest as the best model

Based on the tests conducted, there is sufficient evidence to state that Random Forest was the model that provided the best performance. The images below show the results of the Random Forest classification on the Sentinel-2 and Landsat-8 satellite imageries. The model succeeds in classifying pixels into the appropriate classes. If observed in more detail, with a resolution of 10 meters, the Sentinel-2 imagery displays a smoother classification of road and building objects (built-up areas) and water. Figure 3-6 shows the Random Forest classification results for the Sentinel-2 imagery and Figure 3-7 those for the Landsat-8 imagery.

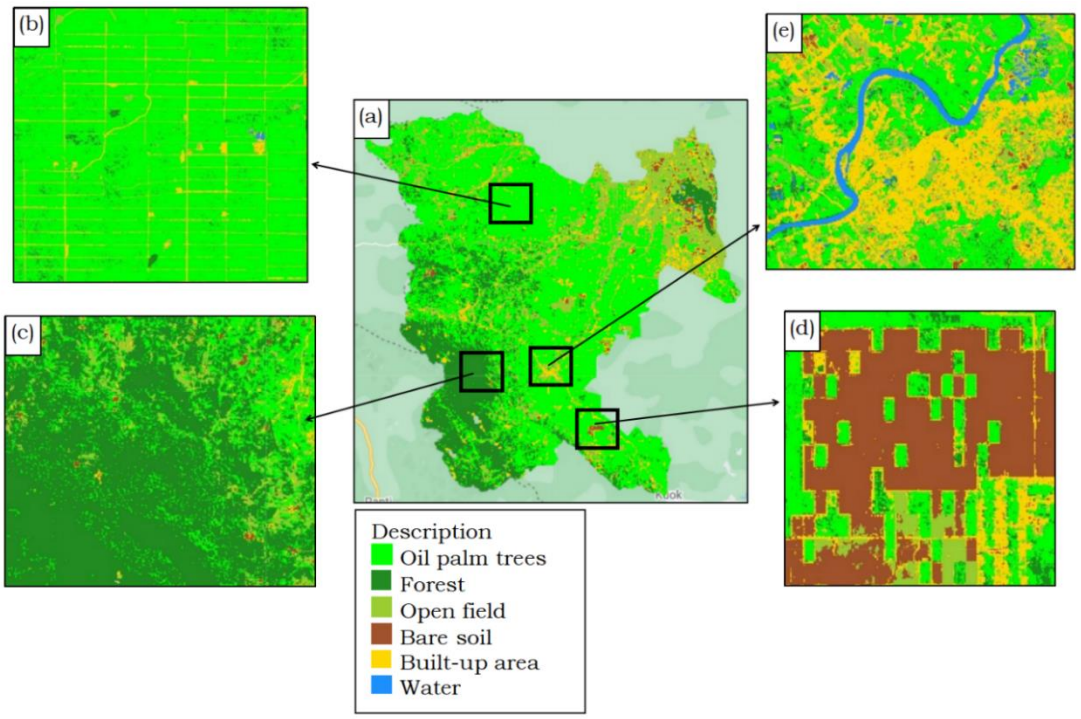

Figure 3-6: Classification results for Sentinel-2 Random Forest.

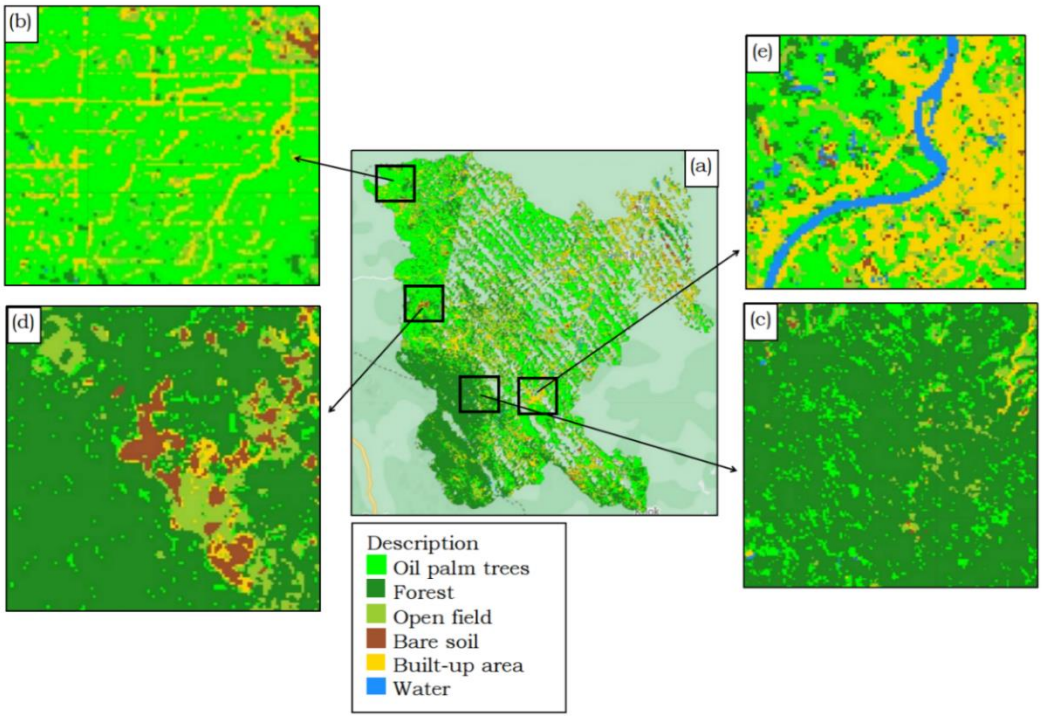

Figure 3-7: Classification results for Landsat-8 Random Forest

4 CONCLUSION

Our study explains the utilisation of Google Earth Engine for providing satellite datasets, and Google Collaboratory Notebook for obtaining classification results of land-cover change at the regional scale, especially for oil palm plantation detection. Various important points can be summarised from the study. (1) The different resolution and cloud cover percentage in the two sets of satellite images affects the accuracy and f1-score results. Sentinel-2, which has a higher resolution and the least cloud cover percentage over the preset time period, achieved the highest accuracy and f1-score of 92%. (2) The combination of RGB, NIR, and SWIR bands with NDVI, EVI, and NDBI indices can provide higher overall accuracy and f-1scores. (3) Random Forest provides the best performance on both optical satellites compared to other classification methods.

However, our study has limitations which provide scope for improvement in further research: (1) combining optical high-resolution imagery satellites to obtain cloud-free land-cover images; (2) finding the most appropriate combination of multispectral bands and composite indices, or even developing a new vegetation index which is able to differentiate the oil palm class; (3) investigating various classification methods by fine-tuning the model hyperparameters in order to increase the overall accuracy and f1-scores.

ACKNOWLEDGEMENTS

The authors would like to thank the journal editors and reviewers for the helpful feedback and suggestions.

AUTHOR CONTRIBUTIONS

Authors: Yunita Nurmasari (YN) and Arie Wahyu Wijayanto (AWY).

YN & AWW conceptualized the research objectives. YN carried out the code writing, experimental simulations, analysis, visualization, and writing original draft preparation. AWW selected the methodology, supervised the project, review and editing the manuscript. All authors have read and agreed to the published version of the manuscript.

REFERENCES

Abdel-Hamid, A., Dubovyk, O., El-Magd, I. A., & Menz, G. (2018). Mapping mangroves extents on the Red Sea coastline in Egypt using polarimetric SAR and high resolution optical remote sensing data. *Sustainability (Switzerland), 10*(3),1–22. doi:10.3390/su10030646

Badan Pusat Statistik (2020). Statistik Indonesia 2020. Badan Pusat Statistik, Indonesia.

Chen, W., Li, X., & Wang, L. (2020). Fine land cover classification in an open pit mining area using optimized support vector machine and world view-3 imagery. *Remote Sensing, 12*(1),12–14. doi:10.3390/RS12010082

Chen, D., Stow, D. A., & Gong, P. (2004). Examining the effect of spatial resolution and texture window size on classification accuracy: an urban environment case. *International Journal of Remote Sensing, 25*(11), 2177-2192. doi:10.1080/01431160310001618464

Dwinita, G., & Murti, S. H. (2016). Aplikasi citra penginderaan jauh untuk estimasi produksi kelapa sawit (elaies guineensis jacq) berbasis Normalized Different Vegetation Index (Perkebunan PT. Mutiara Sawit Seluma, Kabupaten Seluma, Provinsi Bengkulu). *J Bumi Indonesia, 5*(4), 1–12.

Freudenberg, M., Nölke, N., Agostini, A., Urban, K., Wörgötter, F., & Kleinn, C. (2019), Large scale palm tree detection in high resolution satellite images using U-Net. *Remote Sensing, 11*(3), 1–18. doi: 10.3390/rs11030312

Hoeser, T., & Bachofer, F. (2020). Object detection and image segmentation with deep learning on earth observation data : A review — part II : applications. *Remote Sensing, 12*(18), 1–47.doi:10.3390/rs12183053

Lee, J. S. H., Wich, S., Widayati, A., & Koh, L. P. (2016). Detecting industrial oil palm plantations on Landsat images with Google Earth Engine. *Remote Sensing Appl Soc Environ, 4*, 219–224. doi: 10.1016/j.rsase.2016.11.003

Li, L., Dong, J., Tenku, S. N., & Xiao, X. (2015), Mapping oil palm plantations in cameroon using PALSAR 50-m orthorectified mosaic images. *Remote Sensing, 7*(2), 1206–1224. doi:10.3390/rs70201206

Mansor, S. A., & Sarker, M. L. R. (2015). Remote sensing technique for estimating the age of oil palm using high resolution image. *Paper presented at the 36th Asian Conference on Remote Sensing 2015. Phillipines 24-28 October 2015*.

Marsuhandi, A. H., Triscowati, D. W., & Wijayanto, A. W. (2020). Tinjauan pemanfaatan big data penginderaan jauh dan pembelajaran mesin untuk official statistics di wilayah perkotaan. *Jurnal Aplikasi Statistika & Komputasi Statistik, 12*(2), 31–40. doi: 10.34123/jurnalasks.v12i2.282

McCarthy, N., (2020), Which countries produce the most palm oil? Available online. Retrieved 1 Feb 2021, from https://www.statista.com/chart/23097/amount-of-palm-oil-produced-in-selected-countries.

Mubin, N. A., Nadarajoo, E., Shafri, H. Z. M., & Hamedianfar, A. (2019), Young and mature oil palm tree detection and counting using convolutional neural network deep learning method. *Int J Remote Sensing, 40*(19), 7500–7515.doi:10.1080/01431161.2019.1569282

Santucci, E.. (2017). Quantum Minimum Distance Classifier. *Entropy, 19*(12), 659–673. doi:10.3390/e19120659

Shafri, H. Z., Hamdan, N., & Saripan, M. I. (2011), Semi-automatic detection and counting of oil palm trees from high spatial resolution airborne imagery. *International Journal of Remote Sensing, 32*(8), 2095–2115. doi:10.1080/01431161003662928

Solutions HG. (2013). Vegetation analysis: using vegetation indices in ENVI. Retrieved 3 Feb 2021, from http://www.harrisgeospatial.com/Learn/WhitepapersDetail/TabId/802/ArtMID/2

627/ArticleID/13742/Vegetation-Analysis-Using-Vegetation-Indices-in-ENVI.aspx.

Srestasathiern, P., & Rakwatin, P. (2014). Oil palm tree detection with high resolution multi-spectral satellite imagery. *Remote Sensing, 6*(10), 9749–9774. doi:10.3390/rs6109749

Tridawati, A., & Darmawan, S. (2015) Investigation of classification algorithm for land cover mapping in oil palm area using optical remote sensing. *Paper presented at the 1st faculty of industrial technology international congress, Institut Teknologi Nasional, Bandung, 9–11 October 2017.*

Triscowati, D. W., Sartono, B., Kurnia, A., Domiri, D. D., & Wijayanto, A. W. (2019). Multitemporal remote sensing data for classification of food crops plant phase using supervised random forest. *Paper presented at the Sixth Geoinformation Science Symposium, International Society for Optics and Photonicsvol, Yogyakarta, 21 November 2019.*

Triscowati, D. W., Sartono, B., Kurnia, A., Dirgahayu, D., & Wijayanto, A. W. (2020), Classification of rice-plant growth phase using supervised Random Forest method based on Landsat-8 multitemporal data. *Int J Remote Sensing Earth Sci, 16*(2),187–196. doi:10.30536/j.ijreses.2019.v16.a3217

United States Department of Agriculture (2020). Oil Palm World Production. In: Oil Palm Explorer. Retrieved 1 Feb 2021, from http://ipad.fas.usda.gov/cropexplorer/cropview/commodityView.aspx?cropid=4243000.

Vadivelu, S., Ahmad, A., & Choo, Y. H. (2014). Remote sensing techniques for oil palm age classification using Landsat-5 TM satellite. *Sci Int (Lahore) 26*(4),1547–1551.

Wijayanto, A. W., Triscowati, D. W., & Marsuhandi, A. H. (2020). Maize field area detection in East Java, Indonesia : An integrated multispectral remote sensing and machine learning approach. *Paper presented at the 12th International Conference on Information Technology and Electrical Engineering (ICITEE), IEEE, Yogyakarta, 6–8 October 2020.*

Zhang, W., Tan, G., Zheng, S., Sun, C., Kong, X., & Liu, Z. (2018), Land cover change detection in urban lake areas using multi-temporary very high spatial resolution aerial images. *Water (Switzerland), 10*(2), 1–16. doi:10.3390/w10020001.